International Journal of Engineering Trends and Technology
ISSN: 2231–5381 / https://doi.org/10.14445/22315381/IJETT-V73I7P128

Volume 73 Issue 7, 357-368, July 2025

Original Article

Numerical Study on Effect of Entrance Curvature on Blast Valve Location in Duct

Rajeev Jain[1], Pankaj Kumar Sharma[2], Amit Kumar Gupta[3], D R Hipparkar[4]

[1,3,4]*Research and Development Establishment (Engrs), DRDO, Pune, India.*
[2]*Mechanical Engineering Department DIAT, Pune, India.*

[2]*Corresponding Author : rajeev_634@yahoo.com*

Received: 09 December 2024 Revised: 03 July 2025 Accepted: 10 July 2025 Published: 30 July 2025

Abstract - *A passive blast valve is essential for a hardened structure to protect against blast waves. It is mounted on the duct entrance and is designed for a reflective blast wave instead of an incident wave, making it bulky and sluggish when interacting with the blast wave. This study numerically investigates the suitable location of the blast valve for a planar blast wave incident, so that the blast valve may be designed for incident pressure instead of reflective pressure. The study also investigated the effect of different fillet radii of the entrance and conic curves at the entrance curvature on the blast wave propagation in the duct. A Two-Dimensional (2D) model was numerically simulated using LS-DYNA to determine the blast valve location. The duct of a 100 mm section was modeled as a rigid body, and the air domain was a multimaterial ALE. A conical curve was generated for the reference value of 50 mm. It was observed numerically that the peak reflective pressure value reduced substantially in the duct after covering a distance twice that of the duct section.*

Keywords - *Blast valve, Conic curve, Fillet Radius, Entrance curvature, Blast wave propagation.*

1. Introduction

A blast wave is a decaying shock wave generated by the sudden expansion of gases in a small volume. Blast waves carry high energy and can damage the structure or endanger human life, depending on the intensity of the blast waves. Initially, the blast wave is shaped like an explosive, but transforms into a planar wave after traveling a longer distance. Hardened structures are an essential part of the defense against nuclear or explosive blasts. It protects against blast attacks and safeguards personnel and critical equipment. Hardened structures are equipped with air ducts to exchange air with the surroundings to cater to the need to supply fresh air and to remove foul air from the structure. A blast wave carries a large amount of energy, most of which is stopped by the structure. However, blast waves may interact with the air duct of a structure and pass through these openings, potentially causing significant damage to the inside of the structure, life, and equipment based on the intensity of the blast. The incident pressure at the inlet increased due to reflection from the duct surrounding the wall. This causes the equipment installed at the entrance to be designed for reflective pressure rather than incident pressure. It is not known at what distance from the duct entrance the pressure wave reaches close to the incident pressure inside the duct. It is also unknown whether this distance remains constant for different explosive yields. All these points are discussed in this paper using numerical simulations. The equipment and personnel were safeguarded from these blast waves using a blast valve in the air duct. The blast valve is an integral part of the hardened structures. It supplies air under normal conditions and stops the airflow when activated by the operator/sensor (active type) or when the blast wave interacts with it (passive type). Sharma et al. previous work have discussed various blast valves. Passive valves are operated when blast waves interact with the valve.

The same author also explained that a hemispherical plate can take a higher blast load than a flat plate. Figure 1 (a) shows that a passive blast valve with a moving plate against the spring resistance equals the suction pressure developed by the air supply equipment. Air pressure below the plate cannot be greater than 35 kpa [3] overpressure, which is the safe limit of human eardrum operation. When a blast wave strikes the blast valve, the moving plate of the valve closes the path for airflow and safeguards the downward path from any sudden increase in pressure. Similarly, the moving plate moves to the other side to prevent negative pressure inside the structure. After the blast wave subsides, the moving plate returns to its original state. The inertia of the blast valve plays a vital role in the operation of passive-type blast valves. The moving parts are designed based on the intensity of the blast waves. The moving parts of the blast valve should be thick for high-intensity blast waves and thin for low-intensity ones. However, owing to the inertia effect, the high-intensity blast valve response is sluggish for low-intensity blast waves.

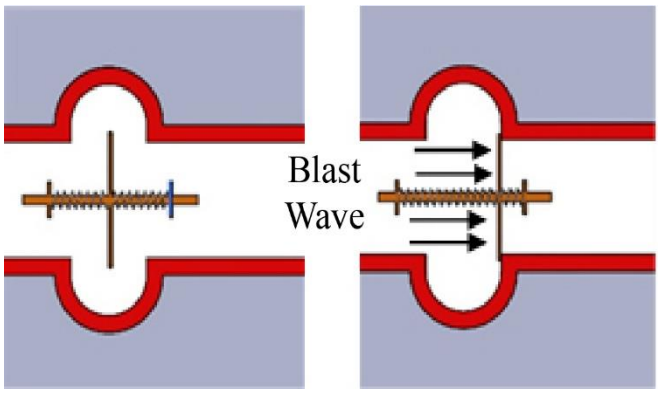

Fig. 1 Blast valve functioning (a) Open valve, and (b) Close valve.

In comparison, high-intensity blast waves may damage the blast valves designed for low-intensity blast waves. A blast valve is generally installed at the duct entrance to protect the other parts used for air exchange, such as filters and blowers, from damage. Blast waves, when arriving at the entrance of the duct and interacting, have two parts: one is incident, and the other is reflective. This made it compulsory to design a blast valve based on the overpressure generated by reflective blast waves, which can reach up to six times [1] the incident pressure in the ideal case. The blast valve design is based on reflective pressure, which makes the blast valve sufficiently bulky to sustain a positive impulse.

This slows the passive valve response owing to mass inertia. Passive valves always act because of their direct interaction with blast waves. However, their location may be a crucial factor in blast protection, which has not been addressed yet. Understanding the optimal location of blast valves is critical for ensuring adequate blast protection. It is also essential to determine the effect of the entrance curvature when determining the blast valve location. Both the problems mentioned above are addressed in the present study using numerical analysis. The analysis was performed without placing a blast valve in the duct. MO Caiyou et al. [2] analyzed passive-type blast valves and found through CFD simulation that the interaction of blast waves with blast valves is sufficient to block the blast wave. Information on various types of blast valves can be found in the literature [3].

The author [4] proposed a new algorithm to modify and improve the blast valve using CFD simulation and experimentation. The author emphasized that the new improved version should be compared with the existing blast valve by benchmarking the existing system. Low pressure drops across the valve for the same flow rate, low impulse residue at the end side of the blast valve, and a decrease in response time are a few parameters that can be compared with the existing blast valve by CFD simulation and corroborated by experimentation. Washington et al. [5] explained a few basic requirements that a blast valve must possess for subterranean shelters, such as being passive to make it independent from other resources, reliable, open for ventilation, and maintenance-free. The author also explained the basic details to be considered while designing the blast valve for subterranean shelter use. A mathematical model was used to determine the closing time of the blast valve and, consequently, the pressure increase inside the shelter. The author also explained that scaling the blast valve can be performed using a dimensional analysis approach by forming 6 pi terms. This helped in designing a large blast valve based on testing a small blast valve on a shock tube. A dimensional multiplication factor can complete the closing time of the scaled valve if the blast valve is scaled only dimensionally and is designed for similar incident pressures and materials.

The authors [6-8]analyzed blast wave propagation in the duct and explained that the blast wave attenuates owing to branching mechanisms and blast wave patterns at the branch junction. All experiments and simulations were performed for closed ducts. During branching, the blast wave is two-dimensional and is again converted into one dimension after traveling a certain distance. The blast wave interactions with structures and their effects can be found in the literature [9-13].

Gnani et al [14] observed that the ramp and symmetric wedge splitter corners show similar results to the rounded corner. The incoming flow is smoothly expanded on the rounded surface compared to the sharp corner. Igra et al. [15] numerically and experimentally analyzed the duct entry of a shock wave, and it was observed that the duct bend or bifurcation attenuated the blast wave through multiple reflections between the walls.

Large-scale structures, such as tunnels, have also been used to examine the blast wave propagation in tunnels. A blast wave is generated by an explosive at the entrance, and its attenuation can be achieved by various means such as obstruction, grooves in the side wall, and other approaches. Eslami et al [16] explained that ‘Y’ and ‘V’ shape obstructions attenuate the blast wave compare to the other 10 types of configurations analyzed. This can be attributed to the larger turbulence zone in the shape discussed. More literature on blast wave attenuation in tunnels can be found in [17-19].

2. Theory

The pressure wave is a time decay phenomenon. The blast wave propagates from the source, and the pressure at a location suddenly increases and then decreases according to Equation (1) at the location. This reduction in pressure does not stop here; it further decreases below the ambient pressure owing to the momentum of the gas particles. Subsequently, it returned to ambient pressure. Equation (1), known as the Friedlander Equation, can explain blast wave propagation with time.

$$P_o = P_b e^{\frac{-t}{t_0}}\left(1 - \frac{t}{t_0}\right) \quad (1)$$

$$P_o = P_b e^{-\beta t}\left(1 - \frac{t}{t_0}\right) \quad (2)$$

This equation was further modified, and Equation (2) was used to identify the peak overpressure and time duration compared with the Friedlander Equation [20].

$$U = \begin{pmatrix} \rho \\ \rho\vec{u} \\ \rho e \end{pmatrix} \quad (3)$$

$$\frac{\partial U}{\partial t} + \vec{\nabla}.F(U) = 0 \quad (4)$$

$$F(U) = \begin{pmatrix} \rho\vec{u} \\ \rho\,\vec{u}\,\vec{u} + p\bar{\bar{I}} \\ (\rho e + p)\vec{u} \end{pmatrix} \quad (5)$$

Where $U = U(\vec{x}, t)$

$$e = \varepsilon + \frac{\overrightarrow{u^2}}{2} \quad (6)$$

Perfect gas equation, where γ>1

$$p = (\gamma - 1)\rho\varepsilon \quad (7)$$

U is an unknown flow variable, and F is the flux component.

u	*Velocity*
ρ	*Density*
p	*Pressure*
e	*Specific total energy*
ε	*Specific Internal energy*
γ	*Ratio of speciifc heat*
F	*Flux Vector*
$\bar{\bar{I}}$	*Identity Tensor*

The blast wave phenomena occur for a very short duration, and in this short time interval, friction losses and heat transfer phenomena can be ignored. This leads to the assumption that the flow is inviscid and time-dependent. The governing equation in Cartesian coordinates for the conservation of mass, momentum, and energy for 2-D is expressed by Equations (3) to (6), along with the perfect gas equation described by Equation (7). These equations were solved using the Finite Element Method. Highly nonlinear transient explicit-based commercial FEM software is available for numerical simulations, and a few examples can be found in [21-23]. LS-DYNA is an explicit-based commercial software used to numerically investigate the effect of blast wave propagation in ducts for different entrance radii. Various methods are available in LS-DYNA to simulate blast wave propagation and its effect on the structure. This study only discussed three methods. The first approach is to make the modeled air domain, structure, and explosive. These methods require propagation of the blast wave to a larger distance, which effectively increases the simulation time. The second approach is to model only the structure; a Load Blast Enhancement (LBE) card can be used, and a blast wave is directly applied to the surface of the structure. This method is unable to provide reflection from the surroundings, which plays an important role in the damage to the structure. It has the advantage of less implementation time. The advantages of the two are combined in the third approach, where only a part of the air domain is made to encompass the structure. Blast waves are imposed on a layer of elements, propagate in air, and interact with the structure. This approach was used in the simulation model. The author [24] compared three approaches (ALE, LBE, and simplified method) used for blast wave simulation and observed that the ALE was closer to the experimental value than the LBE and simplified methods. However, ALE is more computationally intensive and time-consuming than the other two approaches. The pressure and impulse values obtained through LBE were lower than the experimental values. This study followed a hybrid approach, similar to that of the author [24]. LBE and ALE were combined for the initial investigation to provide a trend and acceptable blast-wave simulation results close to ALE [25]. The LBE (LOAD_BLAST_ENHANCED card in LS-DYNA) method was used to simulate the effect of blast wave arrival on the structure [9, 26, 27].

Fluid structure interaction involves the interaction between the fluid and structure, and penalty-based coupling is used in the present model because it conserves energy. The penalty force was measured by node displacement, and correspondingly, the fluid pressure was transferred to the structure. Air was modeled as an ALE element, and a wall as a Lagrangian element. Figure 2 explains the penalty coupling, and Equation (8) provides the penalty coupling force.

$$F_P = k_P * d \quad (8)$$

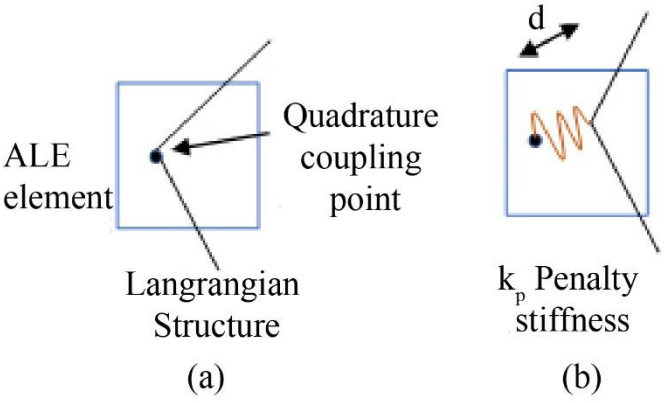

Fig. 2 Penalty coupling explained in (a), and (b)

3. Modelling

A 100 mm duct entrance was made, and fillet radii of 5, 10, 25, 50, and 100 mm were modeled, as shown in Figure 3(a). The conic curves for the three different Rho values were chosen for the simulation. These values are 0.6, 0.5, and 0.4, and according to Solidworks [28], they define a hyperbola, parabola, and ellipse, respectively. The concept of a conic was adopted to make a curve tangent to the duct line. The conic's apex was the line's intersection, as shown in Figure 4(b), and the Rho value was defined as the ratio of the height of the curve to the height of the apex. The value of Rho above 0.5 defines a hyperbola, and below 0.5, the ellipse is equal to 0.5, which represents a parabola. As shown in Figure 4(c), the curve of the 50 mm radius is very close to that of Rho (0.4). The hyperbola curve for the selected Rho(0.6) is the farthest from the circular radius. Four curves (straight, circular, elliptical, and parabolic) were modeled for the analysis. All other parameters were kept the same except for the curvature change at the joint. For the 50 mm configuration, straight lines, circles, ellipses, hyperbola, and parabolas were compared. The numerical model was created in the Ls-Dyna (LS-PrePost 4.8) [29]. The air element was chosen as an ALE (Arbitrary Lagrangian-Eulerian) element because it has the advantage of Eulerian and Lagrangian elements over other elements during the high deformation rate, and the entrance duct was modeled in the shell element. A fixed boundary condition is applied to the shell element (Figure 3). A blast wave was generated using the LS-DYNA LOAD_BLAST_ENHANCE (LBE) model to reduce simulation time. A blast wave was generated by placing 10 kg of TNT 3m away from the entrance duct, and this condition was maintained for all simulations (Figure 3). x. This enabled a comparison of the simulation results for the different entrance curve profiles.

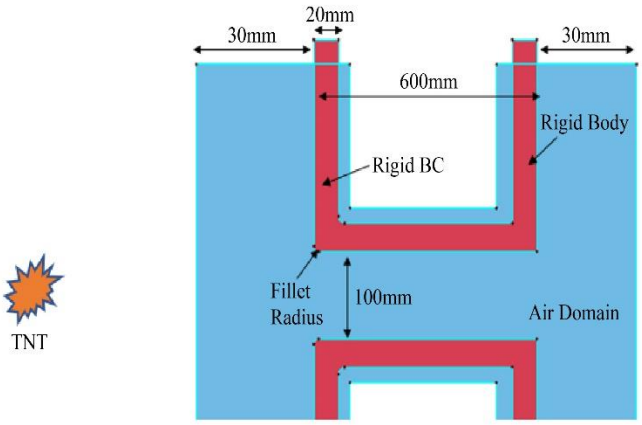

Fig. 3 Model for blast wave simulation

4. Model Validation

The model used was verified with the help of work already carried out by the author [6] in his attenuation study due to a bend in the duct path. The author used a straight duct, 20 mm in width and 50 mm in length, to compare the findings with the bend in the duct. A shock tube was used to verify the effectiveness of the bend duct compared with that of the straight duct.

The experiment was performed with an initial pressure of 101.3kPa, temperature of 294 K, with an incident wave of Mach number 1.2±0.5%. A similar profile was numerically simulated using a mesh size of 0.2 mm. The initial pressure was 100kPa, and the incident wave struck the entrance at Mach number 1.23, using the LBE blast wave generation. The pressure was measured during the original experiment using tracers placed 40 mm and 80 mm downstream from the exit.

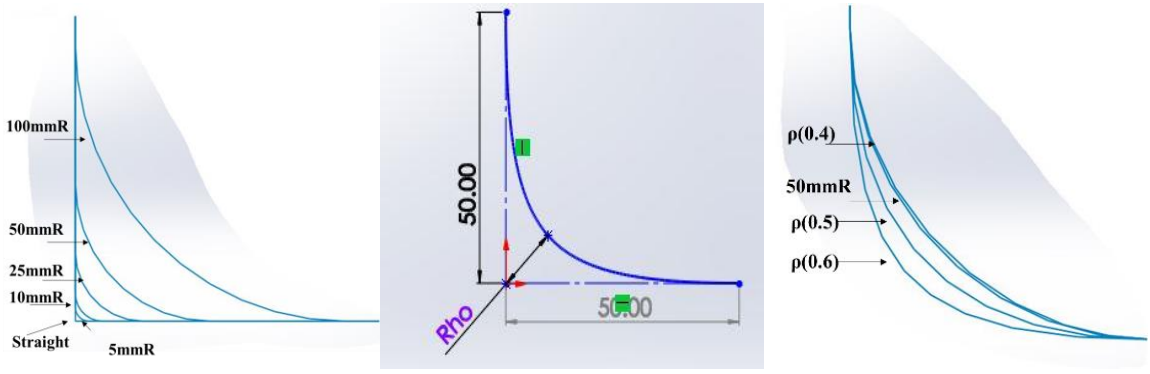

(a) **(b)** **(c)**

Fig. 4 Comparative curve for (a) Fillet radius, (b) Conic construction method, and (c) Conic curve

Table 1. Experimental and numerical results of the straight duct

	Experimental value for straight duct by Igra [6]	Numerically measured	Error
M	1.20	1.23	-2.5%
P1	1.68	1.59	5.21%
P2	1.60	1.57	1.72%

The numerically simulated results show that the variation in the incident Mach number was -2.5%. In comparison, the measured pressure at the location varied from 5.21% to 1.72% at P1 and P2, respectively, within the acceptable limit. The same scheme was followed to measure the blast wave propagation in the duct with varying fillet radius and its result.

5. Mesh Sensitivity Analysis

Mesh sensitivity was analyzed by comparing the pressure value at tracer 1 for a straight curve, as shown in the Table 2. It was observed that a mesh size of 1 mm resulted in a difference of less than 1% in the pressure value at tracer 1 location; thus, the same mesh size was adopted for all simulation purposes.

Table 3 shows that the tracer was placed at intervals to determine the pressure variation at different locations. The positions of these tracers were fixed in all simulations. This enabled the measurement and comparison of pressure at fixed locations. The duct entrance was placed at a fixed location, and only the curvature at the joint was variable. The analysis was performed in 2D. After the mesh optimization, the air mesh size was maintained at 1 mm. The duct was made rigid by fixing its boundary nodes, thereby preventing its nodes from translation and rotation. All curves were compared at a common location from T4 to T7 to check the blast wave profile and the time taken to reach the common point, owing to the different entrance curves. The LS-DYNA cards are used in the numerical analysis setting mentioned in Table 4.

Table 2. Mesh sensitivity analysis

Mesh Size	Incident Pressure (bar) at T1	Error from the previous value
10mm	4.98	-
5mm	5.2	4.42%
4mm	5.26	1.15%
2.5mm	5.34	1.52%
1mm	5.39	0.94%

Table 3. Tracer location

Tracer	T1	T2	T3	T4-T8
Distance (m)	0	0.01	0.05	0.1m Interval

Table 4. LS-DYNA card used in simulation

Material Model	Air -NULL, Duct- Rigid	Air density – 1.19kg/m3
Equation of state	Air- Linear Polynomial	C4, C5- 0.4, E0-2.56e5
Blast wave	Load Blast Enhancement Card	TNT- 10kg Distance from duct entrance - 3m
	Control ALE Card	METH-2, DCT - (-1), PREF – 1.0e5
FSI	*Constrained Lagrange in Solid Card	CTYP-4, DIREC - 2

6. Result and Discussion

For analysis purposes, tracer data were collected at 1e-6 intervals, and d3plot data were stored at 1e-5 intervals to reduce storage requirements, which depend on the model and are influenced by the data interval of the D3plot. The blast wave, which arrives at the duct entrance, has two parts: one that enters the duct, is undisturbed, and the second that strikes outside the duct wall and reflects upward. Part of the reflected wave entered the duct again through diffraction, which was affected by the entrance curvature, blast wave location, and shape, as shown in Figure 5. As shown in Figure 5(a), a straight curve indicates a sharp turn of the diffracted blast wave, which leads it to interact at the middle of the entrance curve owing to symmetry.

The interaction of the diffracted waves occurred at a fillet radius of 5–50 mm at the T4 location (Figure 5 (b-e)). For the 100 mm radius curve, the blast wave was guided by the curvature, and the diffracted wave did not even interact inside the duct at the tracer T4 location (Figure 5 (f)). This subsequently affects the propagation of the undisturbed blast wave that propagates ahead.

The diffracted wave again interacts with the duct wall and reflects. This increases the pressure of the air already processed by the incident blast wave. Multiple reflections occurred owing to the parallel surfaces of the duct, which lost energy owing to friction and moment transfer. Sometimes, this reflected wave intersects the tracer location and increases the pressure locally.

The same can be observed in the graph of the maximum pressure measured at the tracer location. There is a delay in the reflected transition for the fillet radius of 100 mm for the blast wave, as shown in Figures 5(f) and 5(a-e). This difference can also be observed in the time of arrival of the maximum pressure at the tracer location for a fillet radius of 100 mm, as shown in Figure 8, where time is plotted at maximum pressure conditions. A radius of 100 mm resulted in a maximum pressure rise compared to a straight curve. As the blast wave progressed into the duct, the difference between the pressure rises was reduced, as shown in Figure 7(a).

This is attributed to the expansion of the reflected blast waves in the duct, multiple reflections due to the parallel surface of the duct, and the loss of blast wave energy due to friction and momentum transfer. It can also be observed from the time graph that the time of maximum pressure at the location of the tracer is almost the same, except for a 100 mm fillet radius. Maximum pressure from the reflective wave can

be seen after a delay of 0.1ms at tracer location T5 for a fillet radius of 100 mm. This can be attributed to the delay in the arrival of the reflective wave effect at the T5 location, as shown in the pressure-time graph in Figure 7(a). It can be observed that the maximum pressure at tracer location T5 was less than 5 bar for fillet radius below 100 mm. This was almost equal to the incident pressure at the duct entrance. It can be evaluated that the appreciable difference in maximum pressure at tracer location T5 could be traced for 100 mm, 50 mm, and 25 mm fillet radii. For a fillet radius less than 25 mm, the maximum pressure could not be significantly differentiated.

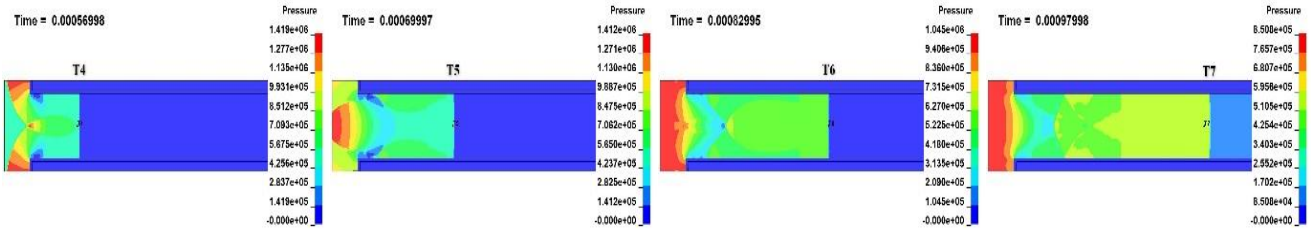

(a)

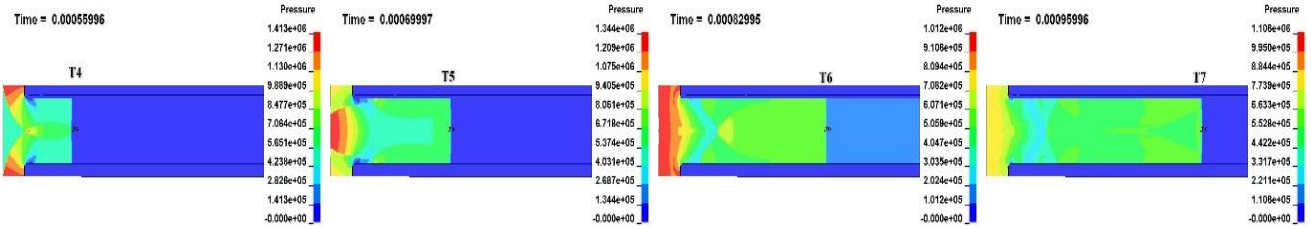

(b)

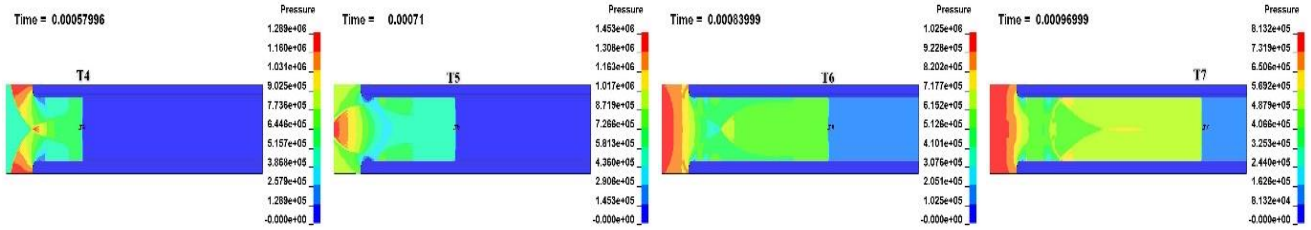

(c)

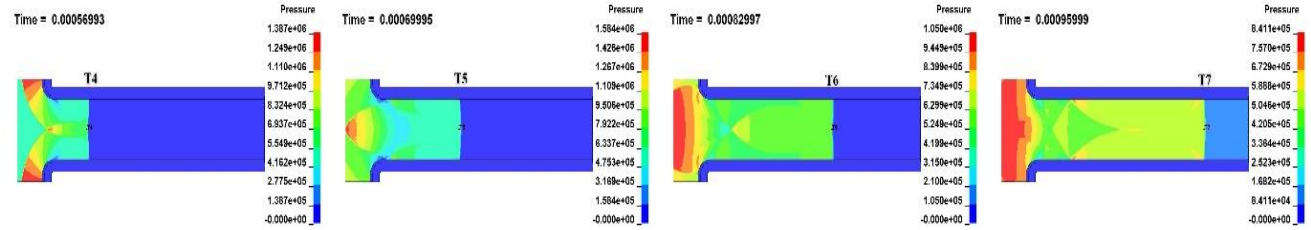

(d)

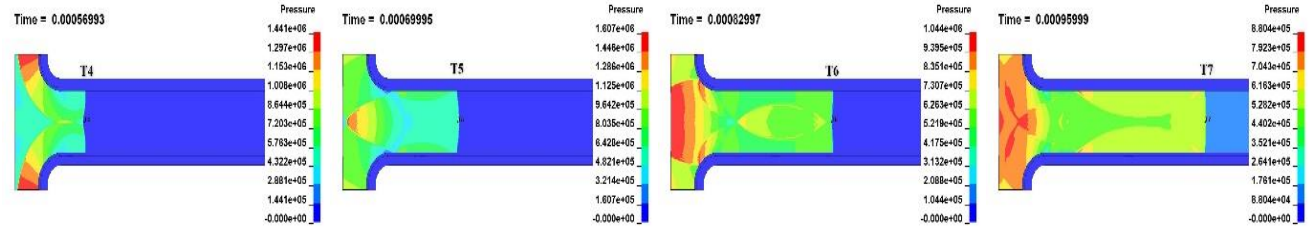

(e)

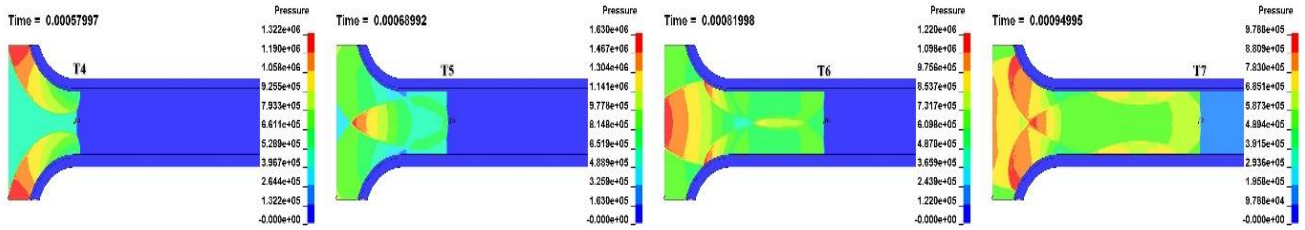

(f)

Fig. 5 Blast wave profile in duct at T4, T5, T6 and T7 (left to right) tracer location for fillet radius (a) 0mm, (b) 5mm, (c) 10mm, (d) 25mm, (e) 50mm, and (f) 100mm

The radius curvature was changed to a conic curve, and the effects of the parabola, ellipse, and hyperbola curvatures were analyzed, as shown in Figure 6, and compared with the circular curvature. The curvature of the conic is defined using the Rho (ρ) value. The hyperbola is defined as Rho >05, and for the ellipse, the value of Rho is less than 0.5. For the parabola, Rho is fixed at 0.5. The relative positions of the different Rho values of the curves are compared in Figure 4(c), and it can be observed that the ellipse ρ(0.4) shape is closer to the circle. The hyperbola ρ(0.6) has the most significant deviation in terms of displacement compared to the fillet radius of 50 mm. It can be interpreted that the hyperbola approaches the intersection point closer than the other conic curves, ρ(≤0.5). The pressure wave locations at the tracer points T4 to T7 are shown in Figure 6.

The pressure wave profiles are similar in Figures 6(a) and (b), whereas Figures 6(c) and (d) show similarities at tracer location T4. Not much can be inferred from the pressure wave profile shown in Figure 6. The maximum pressure values at different tracer locations on the conic curve are plotted in Figure 7(b). The pressure difference was visible only at the T3 location. This can be attributed to the entry of diffracted blast waves inside the duct. At the T3 location, a pressure change occurred owing to the shape of the entrance curvature. The pressure difference between the conic curves was not visible after T5, as shown in Figure 7(b). Maximum pressure at the tracer location is plotted in Figure 8(b). The time of maximum pressure at the tracer location was also not significantly different, as shown in Figure 8(b). The maximum pressure is also close to the incident pressure (4.84 bar) at tracer location T5 for the conic curve.

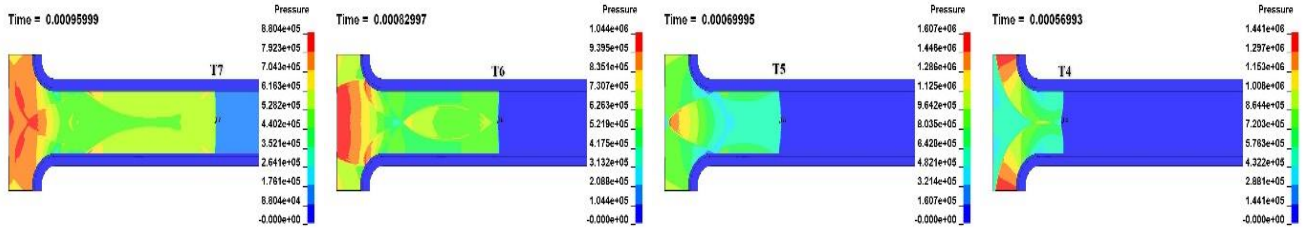

(a)

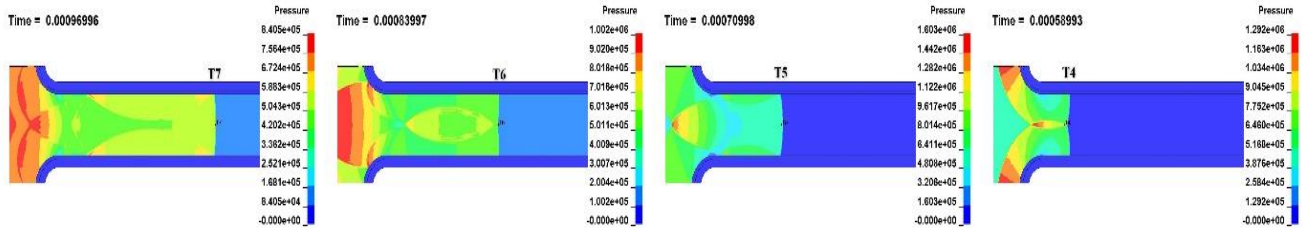

(b)

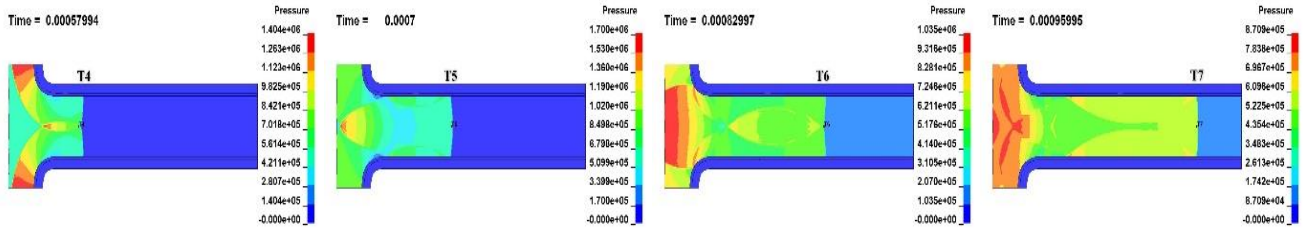

(c)

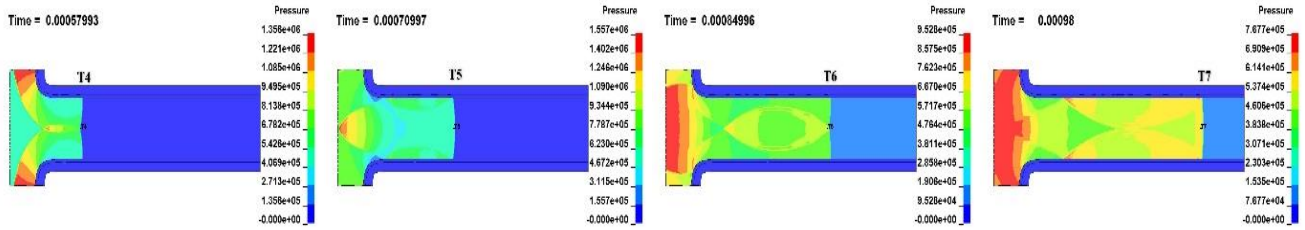

(d)

Fig. 6 Blast wave profile for 50mm fillet radius in duct at tracer locations T4, T5, T6 and T7 (left to right) for fillet curvature (a) Circular, (b) Ellipse (ρ=0.4), (c) Parabola (ρ=0.5), and (d) Hyperbola (ρ=0.6)

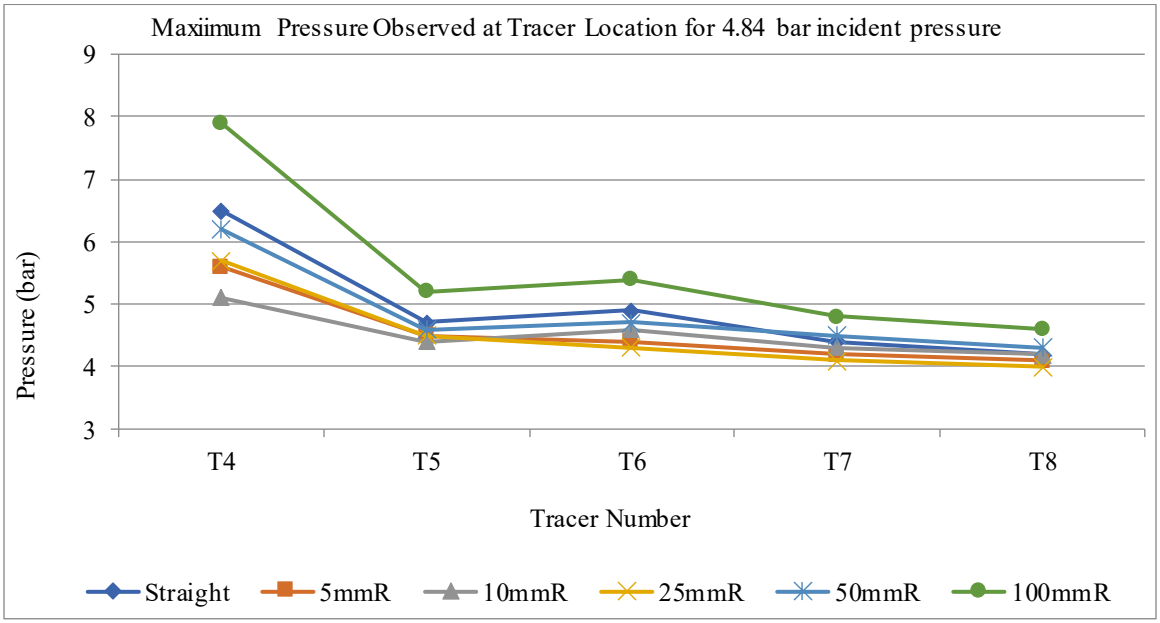

(a)

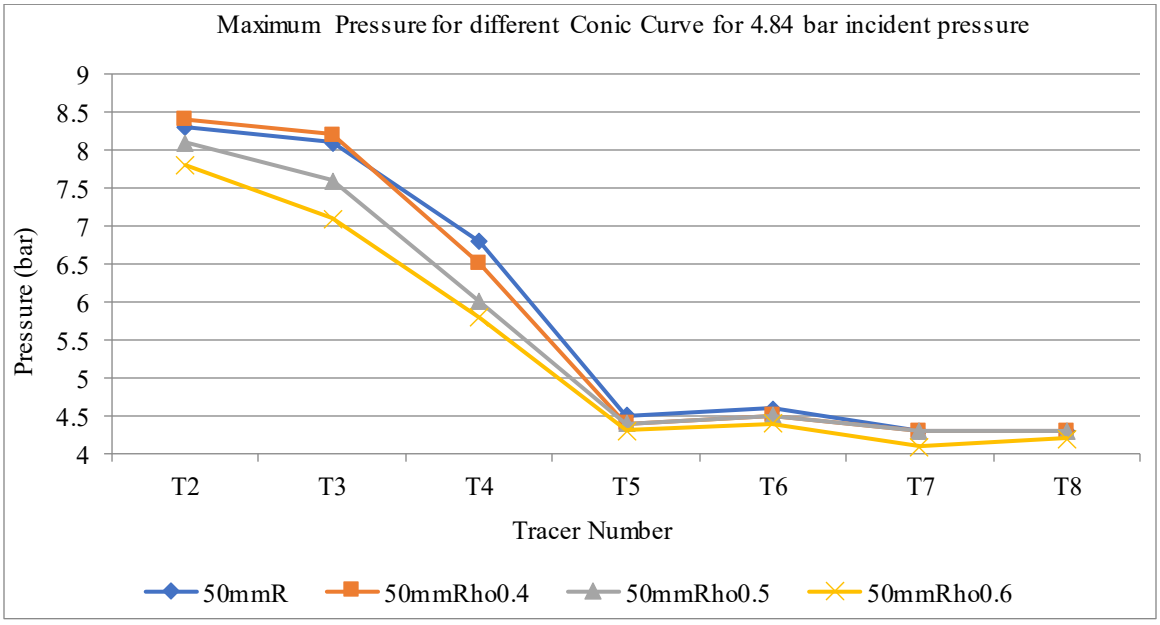

(b)

Fig. 7 Maximum pressure measured at tracer location for curve (a) Straight, and (b) Conic

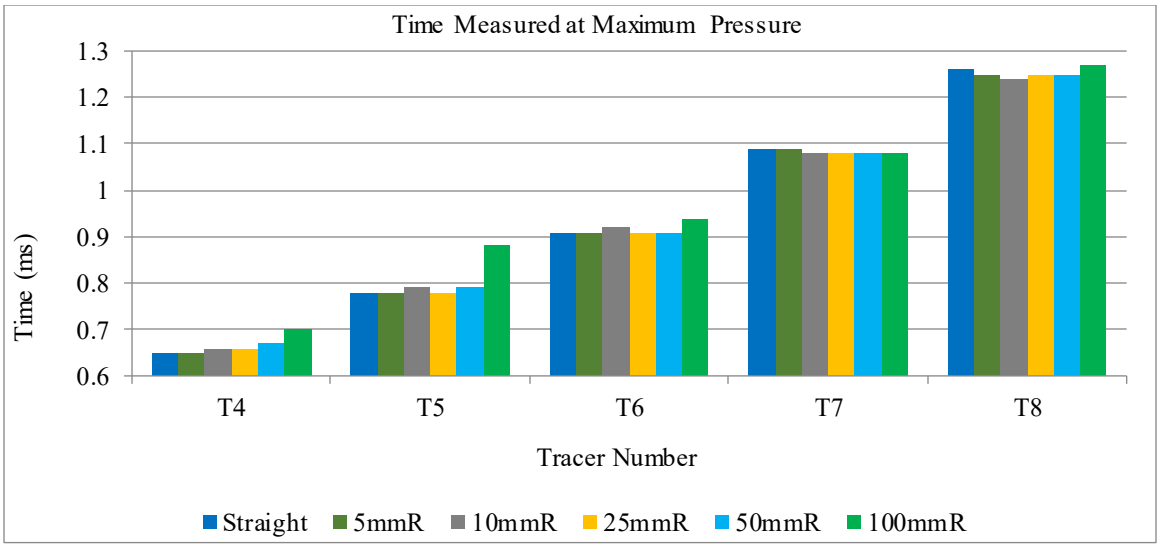

(a)

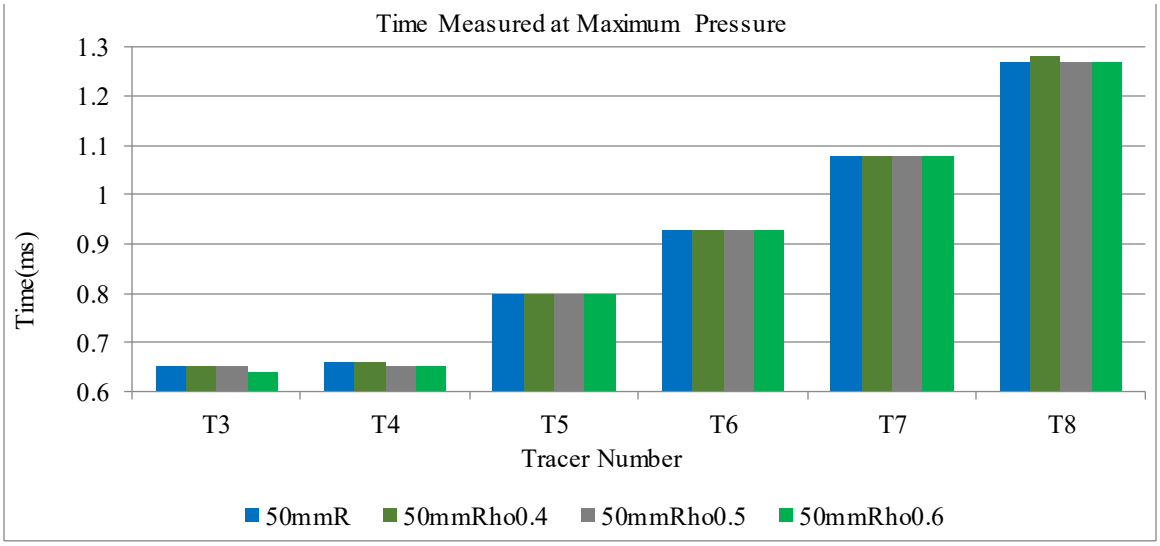

(b)

Fig. 8 Time of arrival of blast wave at tracer location for curvature (a) Straight, and (b) Conic

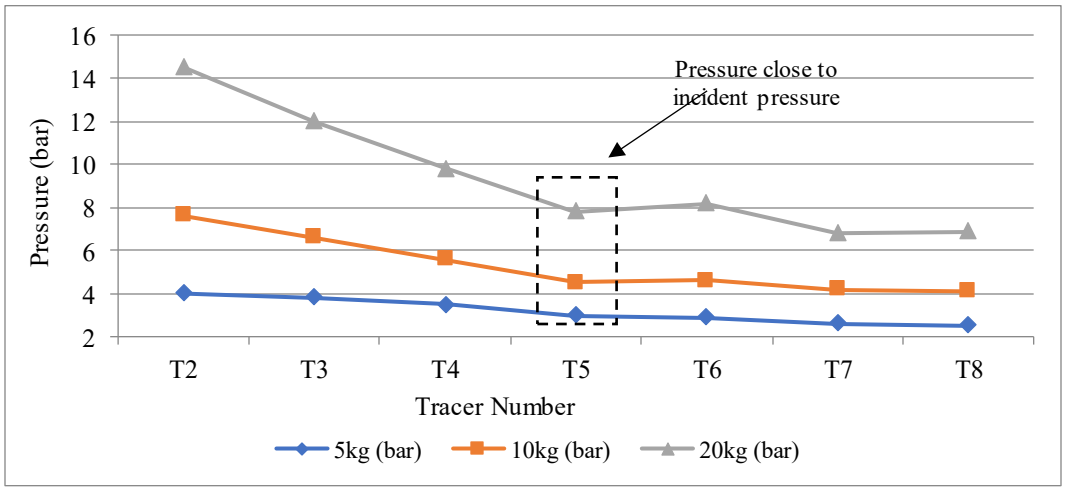

Fig. 9 Maximum pressure at tracer location for 25mm section

A numerical simulation for different scaled distances by varying TNT weights at the same location (3m) was also simulated, and the maximum pressure at the tracer location was plotted for a 25 mm fillet radius, as shown in Figure 9. The maximum pressure observed at the tracer location T5 was close to the incident pressure. It can be interpreted that the maximum pressure approaches the incident pressure at two times the duct cross-section. Figure 10(a-f) plots the pressure history at tracer locations T3–T8 for different fillet radii. At T3, the reflected pressure was higher than the incident pressure.

This happens due to reflected waves from the inner duct. As the wave progressed inside the duct, the intensity of the reflected wave decreased compared with the incident pressure. (Figure 10 (a) to Figure 10(d)). At the tracer locations T7 and T8, the incident pressure was higher than the reflected pressure. The flow became planar again. The same can be observed in Figure 5 for all fillet radii at tracer locations T7 and T8. Tracer locations T5 and T6 can be seen in Figure 10 (c) and (d) as transition points, where a distinct reflected wave is observed and its measured values are close to the incident pressure.

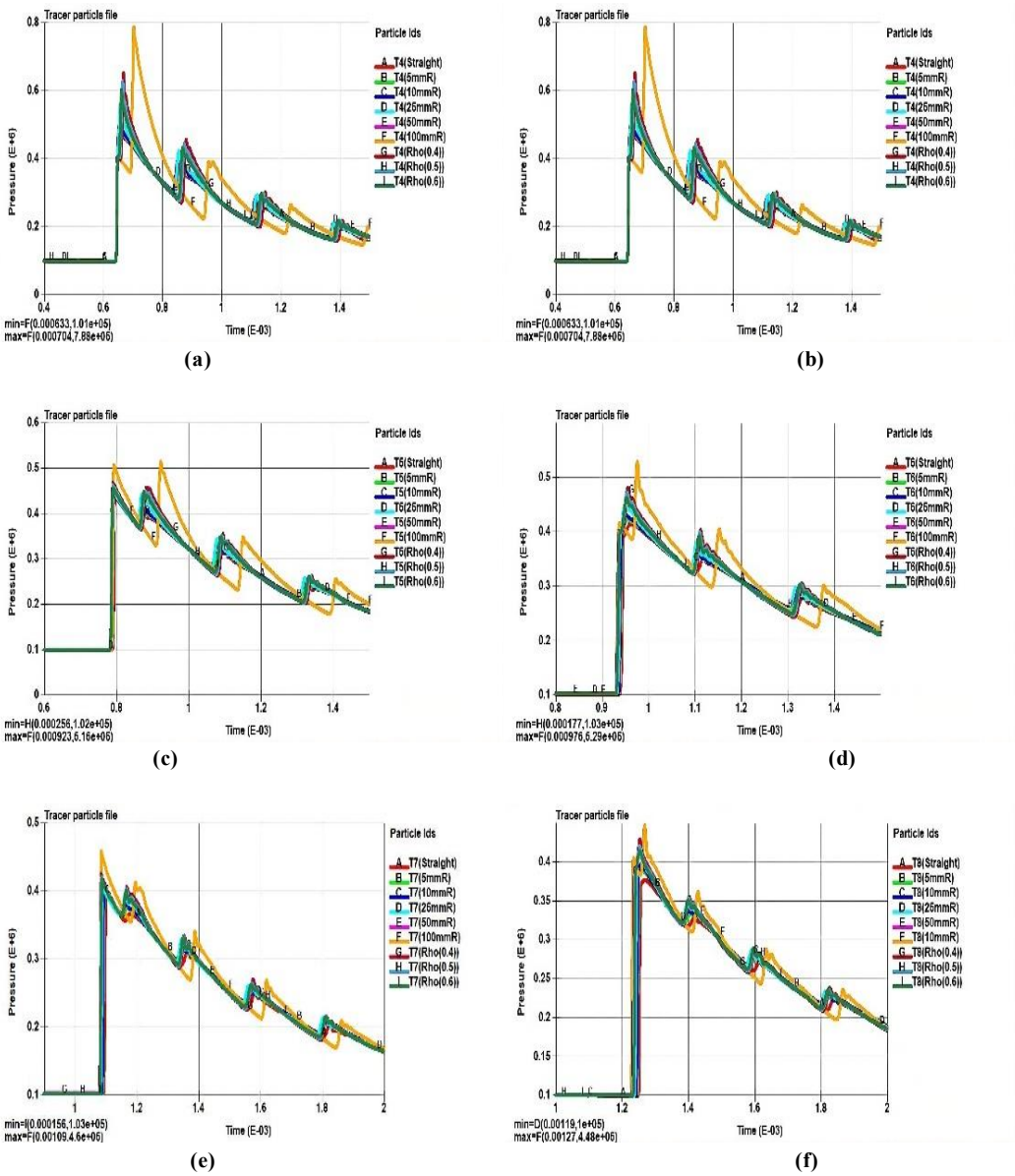

Fig. 10 Pressure history at tracer location (a) T3, (b) T4, (c) T5, (d) T6, (e) T7, and (f) T8

7. Conclusion

From the above analysis, it can be concluded that the overpressure is always more significant than the incident pressure at the duct entrance. The overpressure value decreased as the blast wave progressed in the duct. After covering twice the duct size, the overpressure value was

almost the same as the incident pressure. Further down the duct, the overpressure was reduced. However, a location with a 2 times duct size can be selected for the location of the blast valve or any other equipment for installation. This will aid in the design of a less bulky system.

The effect of the entrance curvature was also analyzed numerically, and it was observed that the overpressure difference among various entrance curvatures below 25 mm and straight curves was almost negligible. The blast valve and other accessories should be installed inside the duct at a distance of at least twice the duct entrance size, with a duct fillet radius of less than one-fourth of the duct size; therefore, the equipment may not be designed for reflective pressure.

The curvature effect on blast wave propagation can be attributed to the blast wave initially getting a larger area for entering the duct and a smooth transition of the reflected wave into the duct owing to curvature. This effect increased with an increase in curvature. The overall impact of a larger entrance curvature is a diffracted blast wave merging deep into the duct, compared to a low entrance curve. A study of oblique incidents of blast waves at the entrance can be analyzed in future work.

References

[1] John Hetherington, and Peter Smith, *Blast and Ballistic Loading of Structures*, CRC Press, 1st ed., pp. 1-336, 2024. [CrossRef] [Google Scholar] [Publisher Link]

[2] Caiyou MO, Xiangwei Zeng, and Kefeng Xiang, "The Passive Blast Protection Valve Flow Field Numerical Simulation and Movement Analysis," *Proceedings of the 4th International Conference on Mechatronics, Materials, Chemistry and Computer Engineering 2015*, Atlantis Press, pp. 482-489, 2015. [CrossRef] [Google Scholar] [Publisher Link]

[3] Blast Valve - 7 Bar Automatic from American Safe Room, American Safe Room (ASR), 2022. [Online]. Available: https://americansaferoom.com/blast-valve/

[4] Lorenz Brenner et al., "Analysis of Pressure Drop and Blast Pressure Leakage of Passive Air Blast Safety Valves: An Experimental and Numerical Study," *Journal of Loss Prevention in the Process Industries*, vol. 75, pp. 1-14, 2022. [CrossRef] [Google Scholar] [Publisher Link]

[5] F. Hughes-Caley, and R. Kiang, "*Blast-Closure Valves*," Defense Technical Information Center, pp. 1-95, 1965. [CrossRef] [Google Scholar] [Publisher Link]

[6] O. Igra et al., "Experimental and Theoretical Study of Shock Wave Propagation through Double-Bend Ducts," *Journal of Fluid Mechanics*, vol. 437, pp. 255-282, 2001. [CrossRef] [Google Scholar] [Publisher Link]

[7] O. Igra et al., "Shock Wave Propagation in a Branched Duct," *Shock Waves*, vol. 8, no. 6, pp. 375-381, 1998. [CrossRef] [Google Scholar] [Publisher Link]

[8] S.M. Mortazawy, K. Kontis, and J. Ekaterinaris, "Normal Shock Wave Attenuation during Propagation in Ducts with Grooves," *Shock Waves*, vol. 30, no. 1, pp. 91-113, 2020. [CrossRef] [Google Scholar] [Publisher Link]

[9] T. Børvik et al., "Response of Structures to Planar Blast Loads - A Finite Element Engineering Approach," *Computers and Structures*, vol. 87, no. 9-10, pp. 507-520, 2009. [CrossRef] [Google Scholar] [Publisher Link]

[10] A. Caçoilo et al., "Structural Response of Corrugated Plates under Blast Loading: The Influence of the Pressure-Time History," *Structures*, vol. 30, pp. 531-545, 2021. [CrossRef] [Google Scholar] [Publisher Link]

[11] Jun Li, and Hong Hao, "A Simplified Numerical Method for Blast Induced Structural Response Analysis," *International Journal of Protective Structures*, vol. 5, no. 3, pp. 323-348, 2014. [CrossRef] [Google Scholar] [Publisher Link]

[12] Xiaoshan Lin, and Mahmud Ashraf, "Pressure-Impulse Response of Semi-Rigidly Connected Steel Plates Under Blast Loading," *International Journal of Protective Structures*, vol. 8, no. 1, pp. 25-57, 2016. [CrossRef] [Google Scholar] [Publisher Link]

[13] R. Rajendran, and J.M. Lee, "Blast Loaded Plates," *Marine Structures*, vol. 22, no. 2, pp. 99-127, 2009. [CrossRef] [Google Scholar] [Publisher Link]

[14] F. Gnani et al., "Experimental Investigation on Shock Wave Diffraction Over Sharp and Curved Splitters," *Acta Astronautica*, vol. 99, pp. 143-152, 2014. [CrossRef] [Google Scholar] [Publisher Link]

[15] D. Igra, and O. Igra, "Simulation of Shock Wave Propagation in a Duct with a Side Branch," *Proceedings of the Institution of Mechanical Engineers, Part G: Journal of Aerospace Engineering*, vol. 228, no. 12, pp. 2226-2236, 2013. [CrossRef] [Google Scholar] [Publisher Link]

[16] Mohammadreza Eslami et al., "Experimental and Numerical Investigation of Blast Wave Attenuation by using Barriers in Different Configurations and Shapes," *Journal of Structural Engineering*, vol. 149, no. 1, pp. 1-22, 2023. [CrossRef] [Google Scholar] [Publisher Link]

[17] Yong Fang et al., "Field Tests on the Attenuation Characteristics of the Blast Air Waves in a Long Road Tunnel: A Case Study," *Shock and Vibration*, vol. 2019, no. 1, pp. 1-11, 2019. [CrossRef] [Google Scholar] [Publisher Link]

[18] Edward Chern Jinn Gan, and Alex Remennikov, "Blast Propagation and Hazard Mapping Outside Coal Mine Tunnels and Shafts," *Tunnelling and Underground Space Technology*, vol. 148, pp. 1-15, 2024. [CrossRef] [Google Scholar] [Publisher Link]

[19] Jingbo Liu, Qiushi Yan, and Jun Wu, "Analysis of Blast Wave Propagation Inside Tunnel," *Transactions of Tianjin University*, vol. 14, no. 5, pp. 358-362, 2008. [CrossRef] [Google Scholar] [Publisher Link]

[20] Isabelle Sochet, *Blast Effects: Physical Properties of Shock Waves*, Springer Cham, 2018. [CrossRef] [Google Scholar] [Publisher Link]

[21] Abaqus, Dassault Systèmes, 2023. [Online]. Available: https://www.3ds.com/products/simulia/abaqus

[22] Ansys LS-DYNA: Multiphysics Solver, Crash Simulation Software, 2021. [Online]. Available: https://www.ansys.com/en-in/products/structures/ansys-ls-dyna

[23] Ansys Autodyn: Short Duration, Severe Loading Simulations, Nonlinear Dynamics Analysis Software, 2021. [Online]. Available: https://www.ansys.com/en-in/products/structures/ansys-autodyn,

[24] M. Abedini et al., "Comparison of ALE, LBE and Pressure Time History Methods to Evaluate Extreme Loading Effects in RC Column," *Structures*, vol. 28, pp. 456-466, 2020. [CrossRef] [Google Scholar] [Publisher Link]

[25] Zahra S. Tabatabaei, and Jeffery S. Volz, "A Comparison between Three Different Blast Methods in LS-DYNA: LBE, MM-ALE, Coupling of LBE and MM-ALE," *12th International LS-DYNA® Users Conference*, pp. 1-10, 2012. [Google Scholar] [Publisher Link] pp. 1-10

[26] Yuzhen Han, and Huabei Liu, "Finite Element Simulation of Medium-Range Blast Loading using LS-DYNA," *Shock and Vibration*, vol. 2015, no. 2, pp. 1-9, 2015. [CrossRef] [Google Scholar] [Publisher Link]

[27] Devon Wilson, Deborah Blass, and Sam Noli, "Implementation of MCEER TR 14-0006 Blast Load Curves in LS-DYNA® and Benchmark to Commonly Practiced Blast Loading Application Methods," *15th International LS-DYNA® Users Conference*, pp. 1-18, 2018. [Google Scholar] [Publisher Link]

[28] Conic Property Manager - 2023 - Solidworks Help, 2023. [Online]. Available: https://help.solidworks.com/2023/english/SolidWorks/sldworks/HIDD_DVE_SKETCH_BCONIC.htm

[29] LS-DYNA Manuals - Welcome to the LS-DYNA Support Site, 2021. [Online]. Available: https://www.dynasupport.com/manuals/ls-dyna-manuals